OPEN

NPG Asia Materials (2015) 7, e212; doi:10.1038/am.2015.96

www.nature.com/am

ORIGINAL ARTICLE

Regulating the coarsening of the γ′ phase in superalloys

Huakang Bian[1], Xiandong Xu[1], Yunping Li[2,3], Yuichiro Koizumi[3], Zhongchang Wang[4], Mingwei Chen[4], Kenta Yamanaka[3] and Akihiko Chiba[3]

The properties of superalloys are typically deteriorated by the coarsening of the nano-sized γ′ phase, which is the primary strengthening component at high temperatures. Stabilizing the γ′ phase represents one of the key challenges in developing next-generation superalloys. Herein, we fabricate a cobalt-nickel-based superalloy with a nanoscale coherent γ′ phase, $(Ni,Co)_3$ (Al,Ti,Nb), which is isolated by stacking-fault ribbons in the alloy matrix as a result of the Suzuki segregation of alloying atoms. Additionally, we demonstrate that this new nanostructure can slow down the coarsening of the γ′ phase at high temperatures. As a result, the cobalt-nickel-based superalloy displays considerably high tensile yield points, exceeding 1650 MPa at room temperature and 1250 MPa at 973 K, which are markedly higher than those of the commonly used nickel- and cobalt-based superalloys. This study thereby paves a new path for developing superalloys with exceptional mechanical performance and thermal stability.
NPG Asia Materials (2015) **7,** e212; doi:10.1038/am.2015.96; published online 28 August 2015

INTRODUCTION

Geometrically close-packed and coherent A_3B-type (A = Ni, Co; B = Al, Ti, and so on) γ′ phases exist in various high-temperature superalloys, and this substantially affects their mechanical performance.[1,2] One of the most critical issues currently restraining the service life of these superalloys lies in the coarsening of the nanoscale γ′ phase upon exposure to high temperatures. To date, much effort has been devoted to probing the morphology of the γ′ phase and to clarifying its coarsening mechanism upon aging in cobalt- and nickel-based superalloys.[3–9] It has been predicted by the Lifshitz-Slyozov-Wagner model[10,11] that coarsening of the γ′ phase in superalloys follows the general relationship $r^3 = kt$, where r is γ′ phase particle radius, t is the aging time and k is the coarsening-related rate constant.

In general, the coarsening of the γ′ phase in superalloys is a diffusion process where large particles grow at the expense of smaller ones in the alloy matrix; this is termed Ostwald ripening.[12–14] The factors that predominantly control the coarsening rate of the γ′ phase include the γ/γ′ phase interfacial energy, the solubility of the γ′ phase in the γ phase and the diffusion coefficient of the constituent elements of the γ′ phase through either the γ/γ′ phase interface or the γ phase matrix.[15] Typical values of the interfacial energy of the γ/γ′ phase have been clearly demonstrated to be $\sim 20\ mJ\ m^{-2}$,[15] a value that is very low and essentially remains stable. In addition, for a given material system, the solubility of small γ′ phase particles and the diffusion coefficient of the constituent elements of the γ′ phase in the homogenous γ phase matrix depend strongly on their compositions, which cannot be substantially lowered by altering the alloy composition. For these reasons, the inhibition of such coarsening remains an open question despite its fundamental importance in enhancing the mechanical properties and thermal stability of superalloys. One key to preserving a high density in the nanoscale γ′ phase while inhibiting its coarsening at high temperatures is to single out an ideal microstructure that can effectively suppress diffusion among γ′ phase particles without sacrificing the strength of the alloy. The formation of planar stacking-fault ribbons in superalloys as a result of the Suzuki segregation of alloying elements may fulfill this role.[16–20] On one hand, the formation of ribbons is energetically preferred because these planar defects lower the stacking-fault energy of the alloys.[17] Furthermore, the rich alloy elements in the ribbons (for example, Mo and Cr in Co-Ni-Cr-Mo alloys) hamper the diffusion of the major elements in the γ′ phase (Ni, Al) across the planar defects, thereby isolating individual γ′ phase nanoparticles.[11,21] On the other hand, the Suzuki segregation of alloying elements itself can serve as an important additional factor in strengthening superalloys at elevated temperatures.[16–18] Herein, we obtain an extremely hard nanoscale γ′ phase of Ni_3X (X = Al, Nb or Ti) in a cobalt-based superalloy composed of 35% Ni, 3% Nb, 2% Al and 0.8% Ti (mass%) and demonstrate that a high density of stacking-fault ribbons can be formed in alloy matrix after cold working and aging at 1023 K as a result of significant Suzuki segregation (Supplementary Figure 1). These results open a new avenue for producing superalloys with

[1]Department of Materials Processing, Graduate School of Engineering, Tohoku University, Sendai, Japan; [2]Department of Materials Science and Engineering, Central South University, Changsha, China; [3]Institute for Materials Research, Tohoku University, Sendai, Japan and [4]Advanced Institute for Materials Research, Tohoku University, Sendai, Japan
Correspondence: Professor Y Li, Department of Materials Science and Engineering, Central South University, Changsha 410083, China.
E-mail: lyping@csu.edu.cn
Received 2 April 2015; revised 22 June 2015; accepted 24 June 2015

extremely high structural thermostability and exceptional mechanical properties.

EXPERIMENTAL PROCEDURES

The ingot of the alloy was prepared by casting a mixture of constituent elements using vacuum induction melting. A solution treatment was performed at 1473 K for 1 h, followed by cooling in Ar gas (labeled as ST). Subsequently, the ingot was cold-swaged from an initial diameter of 13.3 mm to 12.0 mm and 7.72 mm, corresponding to the area reduction rates of 20% (corresponding bar labeled S20) and 66% (S66), respectively. A heat treatment at 1073 K was conducted in a muffle furnace for 3 h and was followed by cooling in air. The aged bars are labeled AG, S20AG and S66AG as listed in Supplementary Table 1.

To investigate the coarsening behavior of the γ' phase at elevated temperatures, discs with a thickness of ~2 mm were cut from the alloys of ST, S20 and S66 perpendicular to the longitudinal axis of the bar. The exposure tests were performed at 1073 K in a muffle furnace in an atmospheric environment. The discs were removed from the muffle furnace and cooled in air after exposure for a certain period.

The H-shaped samples for the tensile tests were prepared by electron-discharge machining with a tensile direction parallel to the longitudinal axis of the rod. The length, thickness and width of the gauge were set to 11.0, 1.0 and 2.0 mm, respectively. The tensile tests were conducted using an INSTRON instrument at room temperature, 573, 773, 973 and 1073 K under an initial strain rate of $1.0 \times 10^{-3}\,s^{-1}$.

To probe the microstructure, the discs were cleaved by electron-discharge machining, ground using grinding paper and polished using an automatic lapping machine. The discs were subsequently etched in a solution of 45% sulfuric acid (H_2SO_4), 43% nitric acid (HNO_3) and 12% phosphoric acid (H_3PO_4) at room temperature at a voltage of 6 V for 15 s. Microstructures were observed using a JEOL JSM-7500F field-emission scanning electron microscope (FESEM, JOEL Ltd., Tendo city, Yamagata, Japan). Analyses of the area fraction and diameter of the γ′ phase were performed using the Image-J software package. X-ray diffraction of the samples was obtained at several stages (AG, S20AG and S66AG). Thin foils for transmission electron microscopy and scanning transmission electron microscopy imaging were prepared by electro-chemical polishing using a twin-jet polisher with a 10% HNO_3 methanol electrolyte at ~243 K. The specimens were then cleaned by an Ar ion sputter beam at 3 kV for 20 min before imaging.

The sharp-tip specimens for the atomic probe tomography were fabricated by cutting the plates into bars of 0.3×0.3 mm using electron-discharge machining, followed by two-step electro-chemical polishing with different concentrations of solution. The polished tips were then investigated by scanning electron microscopy. The scanning electron microscopy-tip profile was used to calibrate the atomic probe tomography reconstruction. Data were acquired with a local-electrode atom probe (LEAP 4000HR, CAMECA, Gennevilliers Cedex, France) equipped with an energy-compensated reflection by which the mass

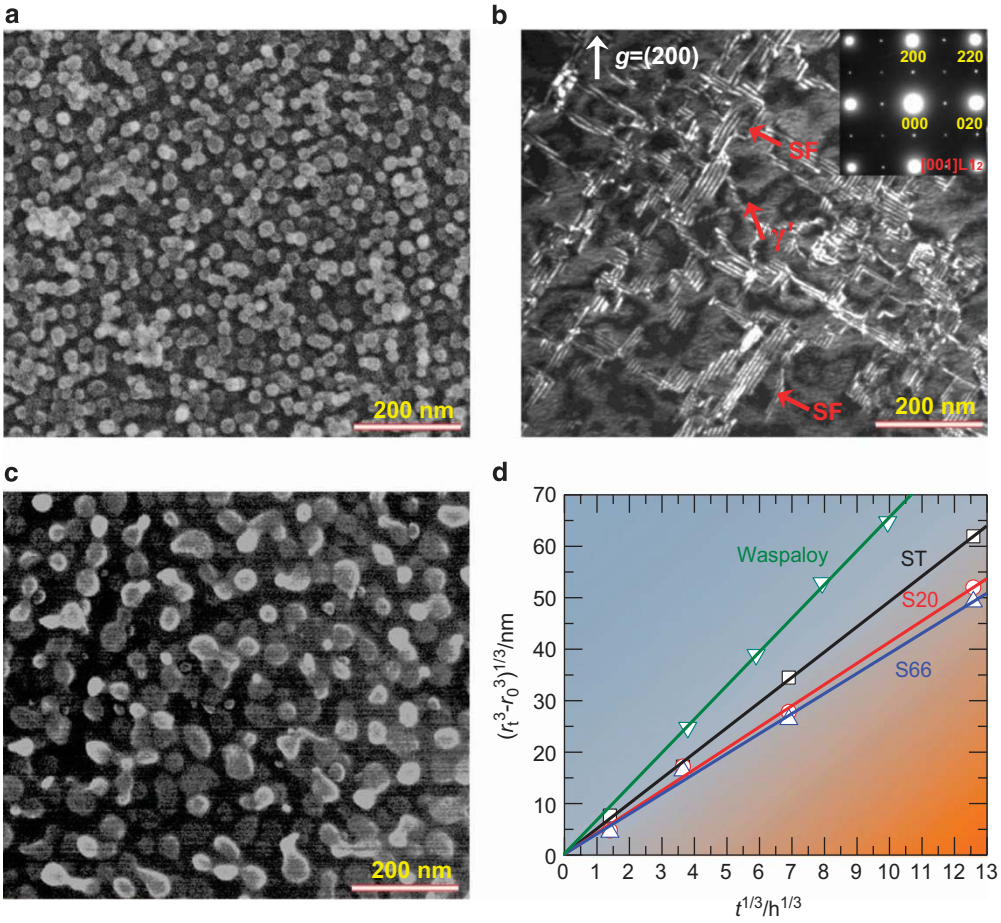

Figure 1 Structural characterization of the alloys. (**a**) Scanning electron microscopy (SEM) image of the Co-35Ni-17.5Cr-8Mo-3Nb-2Al-1.6Fe-0.8Ti alloy cold-swaged by 20%, followed by aging at 1073 K for 3 h (S20AG). (**b**) Weak beam dark-field transmission electron microscopy (TEM) image showing the formation of multilayered stacking-fault ribbons as a result of Suzuki segregation in the S20AG alloy. Inset, the corresponding selected-area diffraction pattern of the S20AG alloy. (**c**) SEM image of the sample cold-swaged by 20%, followed by aging at 1073 K for 2000 h. (**d**) The Lifshitz-Slyozov-Wagner (LSW) relationship illustrating the coarsening of the γ' phase in the solution-treated sample (ST), in the samples cold-swaged by 20% (S20) and 66% (S66AG), and in commercial Waspaloy after subsequent annealing at 1073 K.

resolution was greatly improved. The acquisition temperature was set to 50 K and the pulse frequency and pulse fractions were set to 200 kHz and 20%, respectively. Data processing and 3D atomic reconstruction were performed by CAMECA's integrated visualization and the analysis software (IVAS 3.6.6) package.

RESULTS AND DISCUSSION

Figure 1a shows a scanning electron microscopy micrograph of the Co-35Ni-17.5Cr-8Mo-3Nb-2Al-1.6Fe-0.8Ti (mass%) alloy cold-swaged by 20%, followed by aging at 1073 K for 3 h (named S20AG). The evenly distributed spherical γ′ phases can be readily identified; these have a mean size of ~30 nm and an area fraction of ~60%. Transmission electron microscopy imaging and selected-area diffraction pattern analyses confirm the presence of a γ′ phase with a $L1_2$ structure (Figure 1b). A large number of multilayered stacking faults are also detected along the {111} planes during aging, which are characterized by bright contrast surrounding the γ′ phase in the image (indicated by arrows in Figure 1b). Further studies reveal that the density of these stacking-fault ribbons increases with swaging level and aging time. In contrast, no such planar stacking-fault ribbons are detected in the solution-treated (ST) sample even after prolonged aging, although spherical γ′ phase precipitates are also formed in the ST sample.

To gain insights into the impact of the swaging and aging time, we first apply a swaging of 20% (S20) and an aging time of 2000 h at 1073 K to the alloy, as shown in Figure 1c. Every γ′ phase particle is isolated by multilayered stacking-fault ribbons and grows slightly even after a long aging period, indicating negligible influence of aging time on the coarsening of the γ′ phase. We further establish the Lifshitz-Slyozov-Wagner relationship between the aging time, *t*, and the particle size, *r*, for the γ′ phase in alloys cold-swaged by 20 and 66% (named S20 and S66, respectively) together with those of the ST for comparison (Supplementary Table 1), as shown in Figure 1d. The γ′ phase in both the S20 and S66 samples shows a lower growth rate than that in commercial Waspaloy, Ni-13.2Co-19.4Cr-4.2Mo-1.4Al-2.9Ti (mass%) under comparable aging conditions.[22] The coarsening rate of the γ′ phase is found to decrease significantly after plastic deformation, implying that it relies strongly on the plastic strain. This result, along with the observed microstructure (Figure 1b), implies that the formation of multilayered stacking-fault ribbons as a consequence of Suzuki segregation can obviously retard the coarsening of the γ′ phase.

To shed more light on the spatial distribution of the γ′ precipitates and the alloying elements in the alloy matrix, we performed three-dimensional atomic probe tomography analyses by precisely detecting distribution of the alloying elements in the S20AG alloy. In Figure 2a, the γ′ phase is found to contain mainly Ni, Al, Nb and Ti, and the matrix is composed primarily of Co, Ni, Cr and Mo. Figure 2b shows an isosurface profile of 5.58 at.% Mo, which reveals that the Mo concentration fluctuates in the γ phase matrix. Such fluctuations are also clearly observed in other alloying elements, such as Co and Cr, and were further verified by plotting their concentration profiles across the γ′ phase. The fluctuation can be ascribed to Suzuki segregation in terms of the alloying element-rich, stacking-fault ribbons (Figure 2c). Further quantification of the concentration evolution of the dominant constituent elements in the S20AG alloy (Figure 2d) identifies the composition of the γ′ phase as $(Ni, Co)_3(Al, Nb, Ti)$, in which a small amount of Ni is substituted by Co (Figure 2d). The concentrations of Mo and Cr are much lower in the γ′ phase than in the matrix, and

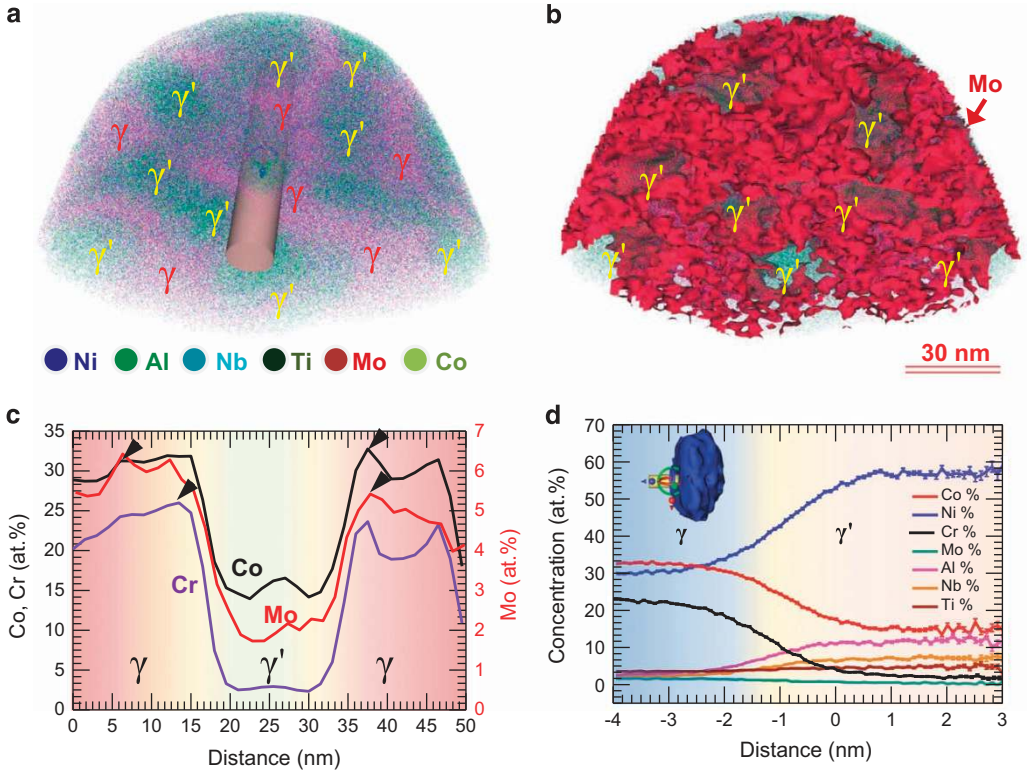

Figure 2 Chemical composition analyses of the alloys. (**a**) Three-dimensional atom probe tomography (ATP) reconstruction of all the alloying elements. The nanoscale γ' phase is found to comprise mainly Ni, Al, Nb, Cr and Mo. (**b**) The isosurface of 5.58 at.% Mo showing the fluctuation of Mo concentration in the alloy matrix. (**c**) Distribution of Mo concentration along the cylinder in (**a**). (**d**) Variation in chemical composition from the γ matrix to the γ′ phase calculated based on the ATP data.

Nb and Ti are also found to be incorporated into the γ′ lattices, stabilizing the structure.[23,24]

Further X-ray diffraction studies determine the lattice constants of the γ and γ′ phases in S20AG to be 0.3588 and 0.3593 nm, respectively (Supplementary Figure 2), which results in a small lattice mismatch of 0.15%. This mismatch is lower than that observed in both nickel-based[5] and cobalt-based superalloys[2] and does not markedly vary with working and aging conditions (Supplementary Table 2). We then conducted high-angle annular dark-field scanning transmission electron microscopy imaging of the S20AG alloy, which reveals clear and bright fringes viewed from the [110] direction (Figure 3a). The bright fringe in the image is identified as a stacking fault because the stacking sequence of the {111} planes across the bright contrast is ABCABABC (Figure 3b). The elemental distributions in the multi-layered stacking-fault ribbons are also probed by energy dispersive X-ray spectroscopy in scanning transmission electron microscopy mode by focusing on a rectangular area in Figure 3a. The elemental maps are derived from the energy dispersive X-ray spectroscopy spectral images acquired from each pixel of 0.2×0.2 nm. From the scanning transmission electron microscopy energy dispersive X-ray spectroscopy mapping, the Co, Cr and Mo elements are found to be enriched, whereas the dominant Nb, Ni and Ti elements in the γ′ phase are found not to be incorporated into the stacking-fault ribbons (Figures 3c,d), which is consistent with the atomic probe tomography observation (Figure 2). In addition, Co and Cr are not symmetrically segregated in the stacking fault, and the segregation of Mo is not as significant as that of Co and Cr.

Like the γ′ phase, the stacking-fault ribbons formed as a result of the Suzuki segregation are also stable at high temperature and may significantly enhance the strength of superalloys by effectively blocking dislocation motion at elevated temperatures.[25] To test this scenario, we conduct tensile tests and show the yield stress (σ_y) as a function of temperature (Figure 4a). The yield stress for both the ST and S66 samples remains nearly constant even when the temperature increases

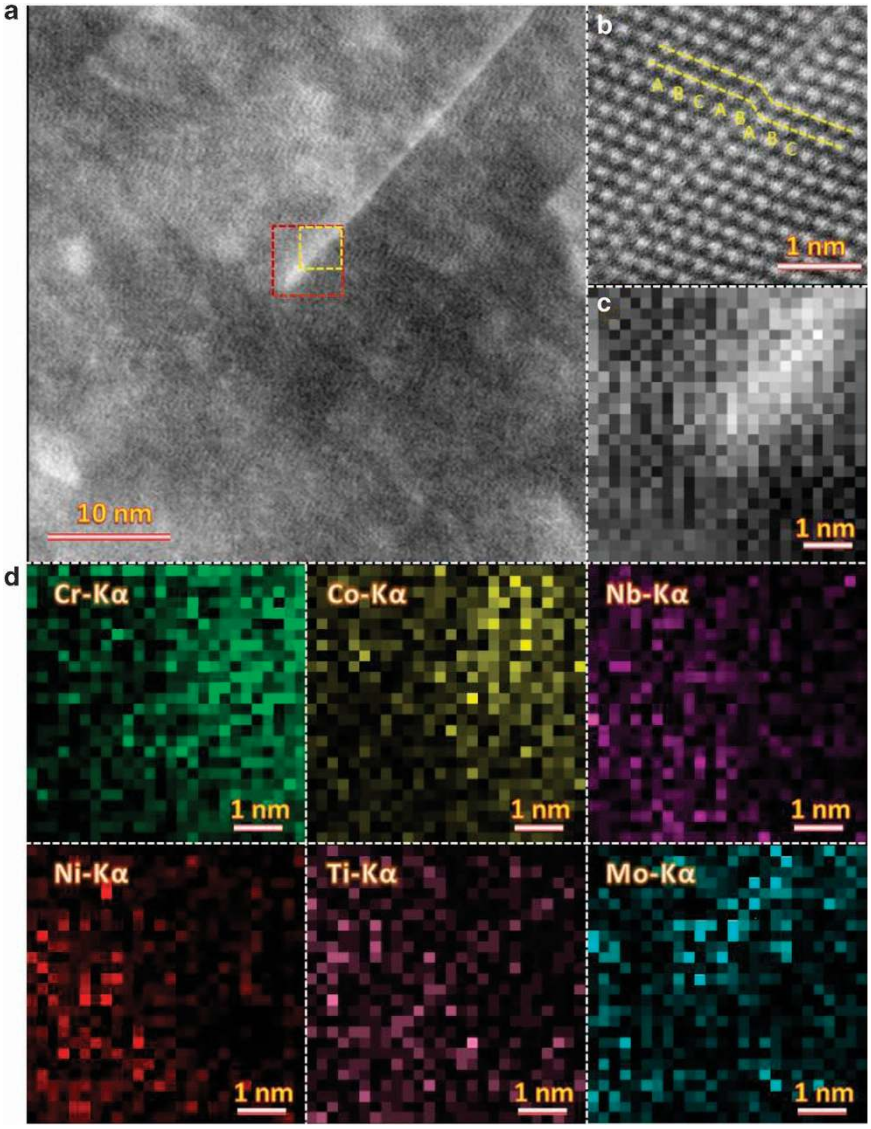

Figure 3 Characterization of stacking-fault ribbons in the S20AG sample. (**a**) High-angle annular dark-field (HAADF) scanning transmission electron microscopy (STEM) image and (**b**) atomic-resolution HAADF STEM image obtained in the yellow rectangular area in (**a**). (**c**) Enlarged HAADF STEM image of the red rectangular region in (**a**). (**d**) Corresponding energy dispersive X-ray spectroscopy elemental mapping of Co-Kα, Cr-Kα, Mo-Kα, Nb-Kα, Ni-Kα and Ti-Kα obtained from a stacking-fault ribbon shown in (**b**).

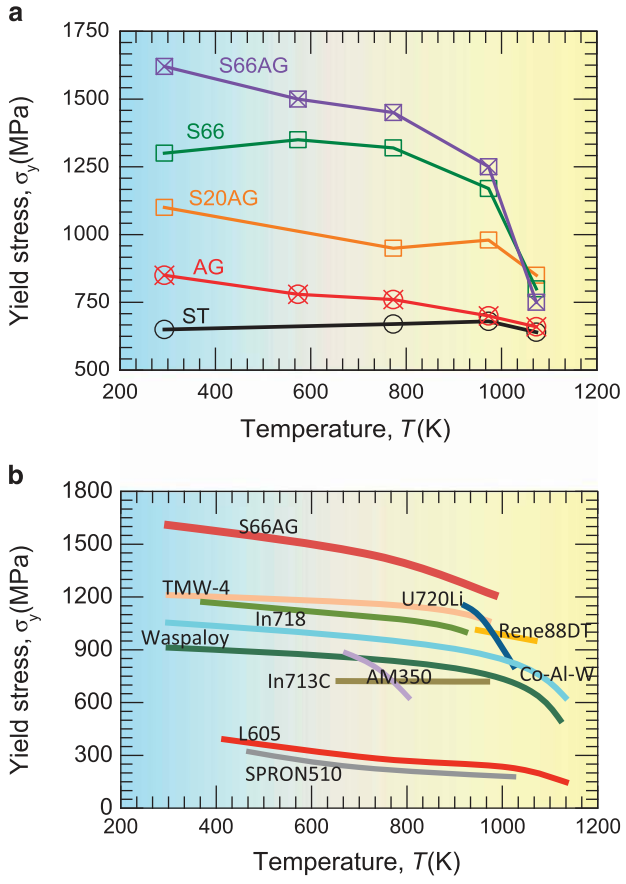

Figure 4 Yield stress as a function of temperature. (**a**) Yield stress for the ST sample, the sample subjected to aging at 1027 K for 3 h (AG), the S20AG sample, the sample swaged by 66% (S66) and the S66 sample subjected to aging at 1027 K for 3 h (S66AG). The stress is measured by tensile test from room temperature to 1073 K. (**b**) Ashby plot showing yielding point as a function of temperature. A comparison is made between a few selected commercial superalloys, TMW-4, Inconel 718, Rene88DT, U720Li, Co-Al-W, AM350, Inconel713C, Waspaloy, L605 and SPRON510 alloy.

to 973 K. However, the yield stress of post-aged AG, S20AG and S66AG samples is markedly increased compared with that of their respective non-aged samples. At a given temperature, the ST sample shows the highest yield stress, followed by the AG, S20AG, S66 and S66AG samples. We thus conclude that both cold working (ST < ∩ S20 < S66) and aging (ST < AG, S66 < S66AG) have critical roles in enhancing the strength of superalloys, indicating that the favorable workability and excellent mechanical performance at room and high temperatures are a synergetic consequence of the γ′ phase and Suzuki segregation. Interestingly, the S66AG sample is found to have a σ_y value of greater than 1650 MPa at room temperature and greater than 1250 MPa at 973 K, which are significantly higher values than those of the currently available major classes of superalloys at the identical temperatures (Figure 4b), demonstrating an advantage of this superalloy over previous ones.

The superior mechanical properties of the present alloy were achieved at both room temperature and elevated temperatures, originating from the synergistic contribution of the fine γ' phase and Suzuki segregation. However, the more surprising result focuses on the slow coarsening of the γ' phase, caused by Suzuki segregation at elevated temperatures. The slower coarsening behavior of the γ' phase is most likely attributable to the situation in which the solute atoms segregate at the stacking-fault ribbons and then become trapped. Meanwhile, these segregated solute atoms change the distribution of not only the constituent solute atoms (Ni, Al, Ti and Nb) of the γ' phase but also the segregated solute atoms themselves. This result indicates that the diffusion of the solute atoms from the shrinking γ' phase to the coarsening one is impeded, whereas the changed distribution results in smaller concentration gradients among the growing and shrinking γ' phases, which provides the driving force for the coarsening γ' phase in superalloys. Although a more detailed investigation is necessary to clarify this mechanism, the fact that the coarsening of the γ' phase is obviously slowed down by Suzuki segregation is academically reliable and valuable.

CONCLUSIONS

The successful combination of alloy-element-rich, stacking-fault ribbons and nanoscale γ′ phases in a superalloy represents a significant step forward in realizing the full potential of superalloys for a broad range of high-temperature applications. Our results demonstrate for the first time that the unique resultant microstructure leads to the effective inhibition of the coarsening of the γ′ phase in superalloys, significantly enhancing their mechanical performance. In particular, we find that the cobalt-nickel-based superalloy displays considerably high tensile yield points exceeding 1650 MPa at room temperature and 1250 MPa at 973 K as a consequence of the nanoscale γ′ phase and planar stacking-fault ribbons, which are markedly higher values than those of the commonly used nickel- and cobalt-based superalloys. Such an outstanding combination of thermal performance in terms of microstructure, mechanical response and ductility holds substantial promise as a new material platform for the further development of high-temperature superalloys.

CONFLICT OF INTEREST

The authors declare no conflict of interest.

ACKNOWLEDGEMENTS

A Chiba and Y Li designed the idea; A Chiba, Y Li, K Yamanaka, Y Koizumi and H Bian designed the experiments. X Xu performed the APT and STEM experiments; H Bian performed all the rest experiments and analyzed the data. H Bian and Y li prepared the manuscript; Z Wang and M Chen revised the grammar; all authors reviewed the manuscript.

1 Kear, B. H. & Thompson, E. R. Aircraft gas turbine materials and processes. *Science* **208**, 847–856 (1980).
2 Sato, J., Omori, T., Oikawa, K., Ohnuma, I., Kainuma, R. & Ishida, K. Cobalt-base high-temperature alloys. *Science* **312**, 90–91 (2006).
3 Ardell, A. J. & Ozolins, V. Trans-interface diffusion-controlled coarsening. *Nat. Mater.* **4**, 309–316 (2005).
4 Meher, S., Nag, S., Tiley, J., Goel, A. & Banerjee, R. Coarsening kinetics of γ′ precipitates in cobalt-base alloys. *Acta Mater.* **61**, 4266–4276 (2013).
5 Kelekanjeri, V. S. K. G., Moss, L. K., Gerhardt, R. A. & Ilavsky, J. Quantification of the coarsening kinetics of γ′ precipitates in Waspaloy microstructures with different prior homogenizing treatments. *Acta Mater.* **57**, 4658–4670 (2009).
6 Tiley, J., Viswanathan, G. B., Srinivasan, R., Banerjee, R., Dimiduk, D. M. & Fraser, H. L. Coarsening kinetics of γ′ precipitates in the commercial nickel base Superalloy René 88 DT. *Acta Mater.* **57**, 2538–2549 (2009).
7 Baldan, A. Review Progress in Ostwald ripening theories and their applications to nickel-base superalloys Part I: Ostwald ripening theories. *J. Mater. Sci.* **37**, 2171–2202 (2002).
8 Baldan, A. Review Progress in Ostwald ripening theories and their applications to the γ′-precipitates in nickel-base superalloys Part II Nickel-base superalloys. *J. Mater. Sci.* **37**, 2379–2405 (2002).
9 Coakley, J., Basoalto, H. & Dye, D. Coarsening of a multimodal nickel-base superalloy. *Acta Mater.* **58**, 4019–4028 (2010).
10 Lifshitz, I. M. & Slyozov, V. V. The kinetics of precipitation from supersaturated solid solutions. *J. Phys. Chem. Solids* **19**, 35–50 (1961).

11 Wagner, C. Theorie der Alterung von Niederschlägen durch Umlösen (Ostwald-Reifung). *Zeitschrift für Elektrochemie, Berichte der Bunsengesellschaft für Phys. Chemie*. **65**, 581–591 (1961).
12 MacKay, R. A. & Nathal, M. V. γ′ coarsening in high volume fraction nickel-base alloys. *Acta Metall. Mater.* **38**, 993–1005 (1990).
13 Voorhees, P. W. The theory of Ostwald ripening. *J. Stat. Phys.* **38**, 231–252 (1985).
14 Kahlweit, M. Ostwald ripening of precipitates. *Adv. Colloid Interface Sci.* **5**, 1–35 (1975).
15 Martin, J. W., Doherty, R. D. & Cantor, B. *Stability of Microstructure in Metallic Systems* 2nd edn. (Cambridge University Press, New York, NY, USA, 1997).
16 Chiba, A. & Kim, M. S. Suzuki segregation and dislocation locking in supersaturated Co-Ni-based alloy. *Mater. Trans.* **42**, 2112–2116 (2001).
17 Koizumi, Y., Nukaya, T., Suzuki, S., Kurosu, S., Li, Y., Matsumoto, H., Sato, K., Tanaka, Y. & Chiba, A. Suzuki segregation in Co–Ni-based superalloy at 973K: An experimental and computational study by phase-field simulation. *Acta Mater.* **60**, 2901–2915 (2012).
18 Otomo, T., Matsumoto, H., Nomura, N. & Chiba, A. Influence of cold-working and subsequent heat-treatment on Young's modulus and strength of Co-Ni-Cr-Mo alloy. *Mater. Trans.* **51**, 434–441 (2010).
19 Asgari, S., El-Danaf, E., Shaji, E., Kalidindi, S. R. & Doherty, R. D. The secondary hardening phenomenon in strain-hardened MP35N alloy. *Acta Mater.* **46**, 5795–5806 (1998).
20 Sorensen, D., Li, B. Q., Gerberich, W. W. & Mkhoyan, K. A. Investigation of secondary hardening in Co–35Ni–20Cr–10Mo alloy using analytical scanning transmission electron microscopy. *Acta Mater.* **63**, 63–72 (2014).
21 Maniar, G. N., Bridge, J. E., James, H. M. & Heydt, G. B. Correlation of gamma-gamma prime mismatch and strengthening in Ni/Fe-Ni base alloys containing aluminum and titanium as hardeners. *Metall. Trans.* **1**, 31–42 (1970).
22 Nakao, Y. & Mitsuhata, K. Behavior of precipitates in Ni-base superalloy, Waspaloy. *Q. J. japan Weld. Soc.* **3**, 815–822 (1985).
23 Rawlings, R. D. & Staton-Bevan, A. E. The alloying behaviour and mechanical properties of polycrystalline Ni3Al (γ′ phase) with ternary additions. *J. Mater. Sci.* **10**, 505–514 (1975).
24 Morinaga, M., Yukawa, N. & Adachi, H. Alloying effect on the electronic structure of Ni3Al (γ'). *J. Phys. Soc. Japan* **53**, 653–663 (1984).
25 Suzuki, H. Segregation of solute atoms to stacking faults. *J. Phys. Soc. Japan* **17**, 322–325 (1962).

Supplementary Information accompanies the paper on the NPG *Asia Materials* website (http://www.nature.com/am)